GEOPHYSICS, VOL. 67, NO. 3 (MAY-JUNE 2002); P. 746–754, 12 FIGS.
10.1190/1.1484517

An integral equation representation of wide-band electromagnetic scattering by thin sheets

Yoonho Song*, Hee Joon Kim‡, and Ki Ha Lee**

ABSTRACT

An efficient, accurate numerical modeling scheme has been developed, based on the integral equation solution to compute electromagnetic (EM) responses of thin sheets over a wide frequency band. The thin-sheet approach is useful for simulating the EM response of a fracture system in the earth. The focus of this development has been the accuracy of the numerical solution over a wide-band frequency range of up to 100 MHz. The effect of displacement currents is included to correctly evaluate high-frequency EM scattering.

Currently, EM responses of two thin sheets with different geometrical and electrical properties embedded in a three-layer earth can be modeled over a frequency band of 10^{-3} to 10^{8} Hz. The layered earth and the sheets can be electrically dispersive. an important feature that allows analysis of frequency-dependent characteristics of the model under investigation. The source field can be generated by a remote or local electric or magnetic dipole located on the surface or in a borehole. A plane-wave source can also be used. and numerical analyses have been made for magnetotellurics and the high-frequency impedance method.

INTRODUCTION

The thin-sheet modeling scheme is an efficient tool that offers valuable insight into a particular class of 3-D electromagnetic (EM) scattering problems such as detecting platelike ore bodies and fluid-filled fractures. Since Price (1949) introduced this innovative approach. various authors (Annan, 1974; Lajoie and West, 1976: Vasseur and Weidelt, 1977; Weidelt, 1981: Walker and West. 1991; Fainberg et al., 1993) have presented numerical implementation of the integral equation formulation.

In modeling platelike structures using the thin sheet, one needs to ensure the conductor is electrically thin (Joshi et al., 1988)-that is, the electric held remains constant through the thickness of the plate. A realistic example of a thin sheet is a laminated vein of ore body in an otherwise layered host rock. A fracture, or a system of fractures, is a commonly encountered geologic feature in environmental and engineering problems and can be represented by a thin sheet. In this case, one can consider the fracture in terms of its admittance, a lumped parameter defined by the product of the thickness and the admittivity (or conductivity under quasi-static conditions) of the fracture. When valid, the thin-sheet approximation reduces the simulation domain to two dimensions. This dramatically reduces memory requirements; as a result, it is possible to compute the EM responses of this important class of models even on a PC.

Following Weidelt*s (1981) elegant formulation for the thin sheet integral equation, we have extended the theory and written an algorithm to include the effect of the displacement currents at high frequencies. Also, we derived an analytic expression for the singular cell.

THIN-SHEET INTEGRAL EQUATION

We consider two sheets embedded in a three-layer earth as shown in Figure 1, The source field can be generated by an electric or magnetic dipole source on the surface or in a borehole. The conductivity and electrical permittivity of host rock and sheets are arbitrary. They can even be dispersive to accommodate frequency-dependent electrical properties described by a Cole-Cole relaxation formula (Cole and Cole, 1941). for example. In the following formulation, we only consider one sheet. Extension of this formula to include multiple sheets is straightforward.

Presented at the 68th Annual Meeting. Society of Exploration Geophysicists. Manuscript received by the Editor May 26. 1999: revised manuscript received June 2001.
*Korea Institute of Geoscience and Mineral Resources, Geoelectric Imaging Lab, 30 Cadging-Dong. Yusung-Gu. Taejon W-350. Korea. E-mall: song@kipam.re.kr.

‡Pukyong National University. Department of Exploration Engineering. 599-l Daeyeon-Dong. Nam-Gu. Pusan 608-737, Korea. E-mail: helkim@ pknu.ac.kr.

**Lawrence Berkeley National Laboratory. Earth Sciences Division. MS 90-1116.1 Cyclotron Rd., Berkeley, California 91720. E-mail: khlee@lbl.gov.

Following Weidelt (1981), we write for the electric field $\mathbf{E}(\mathbf{r})$ at field point $\mathbf{r}$

$$\mathbf{E}(\mathbf{r}) = \mathbf{E}^p(\mathbf{r}) - \hat{z}\int_S \mathbf{G}(\mathbf{r},\mathbf{r}')\cdot\mathbf{J}_S(\mathbf{r}')\,dS'$$

$$= \mathbf{E}^p(\mathbf{r}) - \hat{z}\int_S \mathbf{G}(\mathbf{r},\mathbf{r}')\cdot\tau(\mathbf{r}')\mathbf{E}_S(\mathbf{r}')\,dS', \quad (1)$$

where the integration is over the surface area occupied by the thin sheet, $\mathbf{E}^p(\mathbf{r})$ is the primary electric field in the absence of the sheet, $\mathbf{G}(\mathbf{r},\mathbf{r}')$ is the electric Green's tensor, the subscript S for the electric fields and currents indicates the tangential component, and $\hat{z} = i\omega\mu$ is the impedivity, with ω being the angular frequency and μ being the magnetic permeability assumed to be that of free space. Note that $\mathbf{J}_S(\mathbf{r}')$ is the scattering current in the sheet, which is the product of the tangential component of the total electric field in the sheet $\mathbf{E}_S(\mathbf{r}')$ and the anomalous admittance of the sheet $\tau(\mathbf{r}')$. The anomalous admittance is given by

$$\tau(\mathbf{r}') = \{\Delta\sigma(\mathbf{r}') + i\omega\Delta\varepsilon(\mathbf{r}')\}t, \quad (2)$$

where t is the thickness of the sheet, $\Delta\sigma(\mathbf{r}')$ is the difference in conductivity between the sheet and the surrounding medium, and $\Delta\varepsilon(\mathbf{r}')$ is the difference in electrical permittivity. Expression (1) becomes a Fredholm integral equation of the second kind if the field point $\mathbf{r}$ is on the sheet. If we consider only the tangential component of electric fields, equation (1) is written as

$$\mathbf{E}_S(\mathbf{r}) = \mathbf{E}_S^p(\mathbf{r}) - \hat{z}\int_S \mathbf{G}_S(\mathbf{r},\mathbf{r}')\cdot\tau(\mathbf{r}')\mathbf{E}_S(\mathbf{r}')\,dS'. \quad (3)$$

The subscript S for the Green's tensor indicates the tangential electric field at $\mathbf{r}$ resulting from a scattering current source at $\mathbf{r}'$. The Green's tensor is reduced to a 2×2 dyadic through successive rotation of coordinates about the dip (β) and strike (α) (Zhou, 1989):

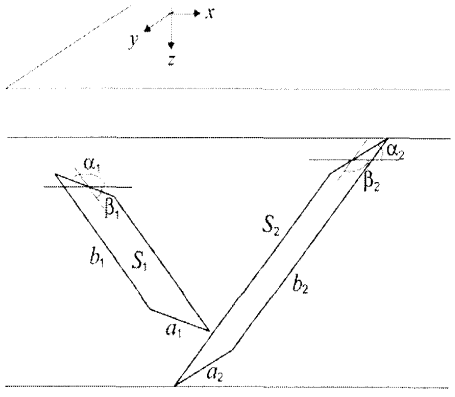

FIG. 1. Geometry of thin sheets embedded in a three-layer earth; a_i, b_i, α_i, and β_i are the strike length, depth extent in the dip direction, strike, and dip angle of the ith sheet, respectively.

$$G_S = \begin{pmatrix} G_{aa} & G_{ab} \\ G_{ba} & G_{bb} \end{pmatrix}$$

$$= \begin{pmatrix} \cos\alpha & \sin\alpha & 0 \\ -\sin\alpha\cos\beta & \cos\alpha\cos\beta & \sin\beta \end{pmatrix}$$

$$\times \begin{pmatrix} G_{xx} & G_{xy} & G_{xz} \\ G_{yx} & G_{yy} & G_{yz} \\ G_{zx} & G_{zy} & G_{zz} \end{pmatrix} \begin{pmatrix} \cos\alpha & -\sin\alpha\cos\beta \\ \sin\alpha & \cos\alpha\cos\beta \\ 0 & \sin\beta \end{pmatrix}. \quad (4)$$

Integration of Green's tensor may impose a significant numerical instability for a resistive host or small propagation constant since every element has a term divided by the propagation constant, as shown later. To solve this problem, Weidelt (1981) uses the Helmholtz theorem to write the vector vanishing at infinity as the sum of nonrotational and solenoidal components. Separating the Green's tensor into numerically stable parts and defining the scattering current in the sheet as the sum of the divergence-free induction current part and the curl-free conduction current or current channeling part, Weidelt's (1981) approach may be generalized as

$$\mathbf{G}_S(\mathbf{r},\mathbf{r}') = \mathbf{S} + \tfrac{1}{k_j^2}\nabla_S\boldsymbol{\Phi}, \quad (5)$$

$$\mathbf{J}_S(\mathbf{r}) = \nabla_S\times(\hat{\mathbf{c}}\psi) + k_j^2\nabla_S\varphi, \quad (6)$$

$$\hat{\mathbf{c}} = \hat{\mathbf{a}}\times\hat{\mathbf{b}}, \quad (7)$$

and

$$\nabla_S = \frac{\partial}{\partial a}\hat{\mathbf{a}} + \frac{\partial}{\partial b}\hat{\mathbf{b}} = \left(\cos\alpha\frac{\partial}{\partial x} + \sin\alpha\frac{\partial}{\partial y}\right)\hat{\mathbf{a}}$$

$$+\left(-\sin\alpha\cos\beta\frac{\partial}{\partial x} + \cos\alpha\cos\beta\frac{\partial}{\partial y} + \sin\beta\frac{\partial}{\partial z}\right)\hat{\mathbf{b}}, \quad (8)$$

where the propagation constant at the jth layer is

$$k_j = \sqrt{\omega^2\mu\varepsilon_j - i\omega\mu\sigma_j} \quad (9)$$

and where $\hat{\mathbf{a}}$ and $\hat{\mathbf{b}}$ are the unit vectors in the direction of strike and dip, respectively. The terms $\mathbf{S}$ and $\nabla_S\boldsymbol{\Phi}$ are to be determined in a layered earth using boundary conditions and the reciprocity principle. The vortex current $\nabla_S\times(\hat{\mathbf{c}}\psi)$ is confined to the sheet so that the potential ψ may be taken as constant along the edge of surface S. Substituting equations (5) and (6) into equation (3), the integral of the term containing $1/k_j^2$ vanishes and the integral equation reduces to

$$\mathbf{E}_S(\mathbf{r}) = \mathbf{E}_S^p(\mathbf{r}) - \hat{z}\int_S \{\mathbf{S}\cdot\nabla'_S\times(\hat{\mathbf{c}}\psi)$$

$$+ (k_j^2\mathbf{S} + \nabla_S\boldsymbol{\Phi})\cdot\nabla'_S\varphi\}\,dS'. \quad (10)$$

This formulation is suitable for modeling EM responses of sheets over a wide range of frequencies in a layered earth of arbitrary electrical properties. Equation (10) can be discretized into a system of equations by dividing the sheet into a number

of cells of constant admittance, the size of each cell being small enough to assume a constant scattering current within the cell:

$$\sum_{k=1}^{N}\left\{\left(\delta_{k,l}\mathbf{I}+\hat{z}\tau_l\int_{S_k}\mathbf{S}\,dS'\right)\cdot[\nabla'_S\times(\hat{\mathbf{c}}\psi_k)]+\left[k_j^2\delta_{k,l}\mathbf{I}+\hat{z}\tau_l\int_{S_k}\left(k_j^2\mathbf{S}+\nabla_S\mathbf{\Phi}\right)dS'\right]\cdot(\nabla'_S\varphi_k)\right\}=\tau_l\mathbf{E}^p{}_{s,l},\qquad l=1,2,\ldots,N=N_a\times N_b. \tag{11}$$

Hence, the scattering current or the tangential electric field in each cell of the sheet is calculated by first solving equation (11) for the potentials ψ and φ and then approximating each component by curl and gradient of potentials at four corner points of each cell:

$$\begin{aligned}\tau E^a_{i,j}&\approx\frac{1}{2\Delta_b}(\psi_{i-1,j}-\psi_{i-1,j-1}+\psi_{i,j}-\psi_{i,j-1})+\frac{k_j^2}{2\Delta_a}(\varphi_{i,j-1}-\varphi_{i-1,j-1}+\varphi_{i,j}-\varphi_{i-1,j}),\\ \tau E^b_{i,j}&\approx\frac{-1}{2\Delta_a}(\psi_{i,j-1}-\psi_{i-1,j-1}+\psi_{i,j}-\psi_{i-1,j})+\frac{k_j^2}{2\Delta_b}(\varphi_{i-1,j}-\varphi_{i-1,j-1}+\varphi_{i,j}-\varphi_{i,j-1}),\end{aligned} \tag{12}$$

where

$$\Delta_a=\frac{a}{N_a},\qquad \Delta_b=\frac{b}{N_b}.$$

There are $2N_aN_b$ independent linear equations because the tangential electric field on the sheet is represented by only two directional components in $\hat{\mathbf{a}}$ and $\hat{\mathbf{b}}$. The number of unknowns, which are potentials ψ and φ at each nodal point of the cell, is actually $(N_a+1)\times(N_b+1)$. A closer look at the nature of the potentials makes it possible to avoid this computational inconsistency. Since the potential of the divergence-free part ψ is constant along the edge of the sheet, by setting all the edge values to be zero, only $(N_a-1)\times(N_b-1)$ values must be calculated. Also, because only the derivatives of potentials φ are necessary in equation (11), the resultant tangential electric fields remain unchanged when a constant is added to the potential. In addition, since the numerical evaluation of the gradient in equation (12) always includes the pair of even and odd orders of i and j, one can select two arbitrary constants which have no effect on the results. A convenient set of constants is (Weidelt, 1981)

$$\varphi_{N_a+1,N_b}=\varphi_{N_a+1,N_b+1}=0. \tag{13}$$

Consequently, the total number of unknowns becomes equal to the number of linear equations.

The resultant EM fields at receiver locations are represented as

$$\mathbf{E}(\mathbf{r})=\mathbf{E}^p(\mathbf{r})-\hat{z}\sum_{k=1}^{N}\tau_k\int_{S_k}\mathbf{G}(\mathbf{r},\mathbf{r}')\,dS'\cdot\mathbf{E}_S(\mathbf{r}_k) \tag{14}$$

and

$$\mathbf{H}(\mathbf{r})=\mathbf{H}^p(\mathbf{r})-\hat{z}\sum_{k=1}^{N}\tau_k\int_{S_k}\nabla\times\mathbf{G}(\mathbf{r},\mathbf{r}')\,dS'\cdot\mathbf{E}_S(\mathbf{r}_k). \tag{15}$$

In a layered earth, Green's tensor is generally represented by potentials with TE and TM modes of polarization (Ward and Hohmann, 1988) and can be separated into a whole space and layered-earth parts. Each element of the whole-space Green's tensor can be calculated accurately using the closed-form formula. The integration of Green's tensor elements over the cell is done numerically using Simpson's rule or Gaussian quadrature, according to the order of derivatives of the kernels. Numerical difficulty arises at the singular cell at which $\mathbf{r}=\mathbf{r}'$. Since the scalar Green's function becomes larger as $\mathbf{r}$ gets closer to $\mathbf{r}'$, accurate evaluation of the singular integral is the most important factor determining the accuracy of the integral equation modeling. Note that the scalar Green's function is symmetric about the singular point. We therefore replace the square singular cell with a circular disk of the same area. It is known that the singular cell integrals have closed-form results:

$$\int_{S_0}\frac{e^{-ik|\mathbf{r}-\mathbf{r}'|}}{4\pi|\mathbf{r}-\mathbf{r}'|}dS'\cong\frac{i}{2k}(e^{-ik\rho_0}-1) \tag{16}$$

and

$$\int_{S_0}\frac{\partial^2}{\partial a^2}\frac{e^{-ik|\mathbf{r}-\mathbf{r}'|}}{4\pi|\mathbf{r}-\mathbf{r}'|}dS'=\int_{S_0}\frac{\partial^2}{\partial b^2}\frac{e^{-ik|\mathbf{r}-\mathbf{r}'|}}{4\pi|\mathbf{r}-\mathbf{r}'|}dS'\cong-\frac{(1+ik\rho_0)e^{-ik\rho_0}}{4\rho_0}, \tag{17}$$

where ρ_0 is the radius of the circular disk and the integral of cross-derivative terms vanishes.

Evaluation of the layered-earth Green's tensor and its integration over the cell is also done numerically. The Green's tensor elements can be represented by Hankel transforms (Ward and Hohmann, 1988) and are usually evaluated numerically using digital filtering techniques. In the high-frequency range, highly oscillatory kernels associated with displacement currents often cause the digital filtering techniques to fail. We used a numerical algorithm using Gaussian quadrature and continued fractions by Chave (1983) with a modification to accommodate the branch-cut integral when the source or receivers are located in the air. When the displacement current is taken into account, since the wave propagation constant is real in the air, there exists a zero vertical wavenumber $u_0=\sqrt{\lambda^2-k_0^2}$ when we integrate the kernel from zero to infinity along the real axis of horizontal wavenumber λ. Considering all the kernels have the vertical wavenumber in the denominator, we split the Gaussian quadrature integral into two parts by the branch point $\lambda=k_0$ and sum the two separate results.

ACCURACY TESTS

We have developed a numerical code, HFSHEET, based on the algorithm described above. The performance of the modeling code is first verified by comparing it with the PLATE program (Dyck et al., 1980). Figure 2 shows the model used in Zhou (1989) and the results of both codes. A conductive square sheet of 100×100 m is located in free space, symmetrical about the plane defined by the boreholes. The target conductance is 1.0 S, and the operating frequency is 1.0 kHz. A vertical magnetic dipole source is at 50 m depth, and secondary vertical magnetic fields are gathered along the receiving borehole. In the

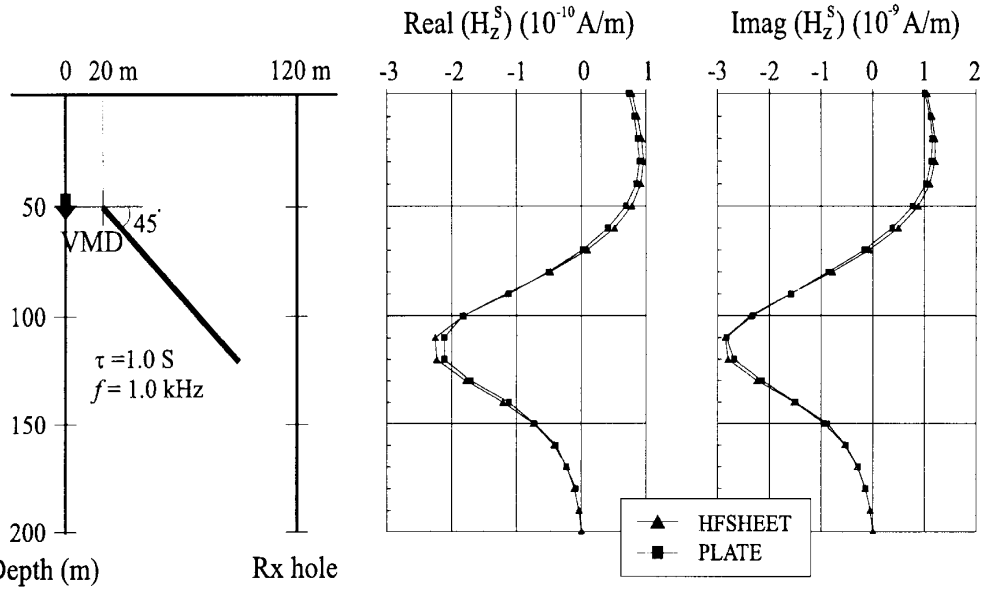

FIG. 2. Free-space responses compared with PLATE (Dyck et al., 1980). The thin sheet is 100 × 100 m and has 1.0 S conductance located in a free space and symmetrical about the plane defined by the boreholes. A vertical magnetic dipole source is at 50 m depth, and secondary vertical magnetic fields are measured along the receiving (Rx) borehole. The model used and the Plate results are from Zhou (1989).

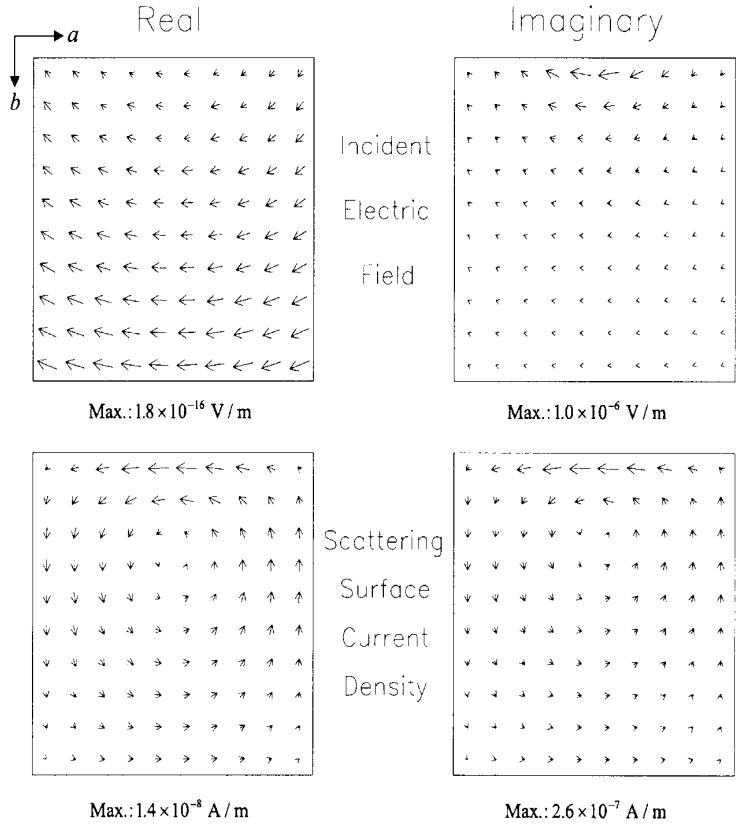

FIG. 3. The directions and amplitudes of incident electric fields and scattering surface currents on the sheet for the results in Figure 2. The incident fields show a radiation pattern of electric fields generated by the magnetic dipole source, while the scattering currents show vortex currents since there is no current leakage from the sheet into the insulating free space.

computation with HFSHEET, the thin sheet is divided into 10×10 cells; four eigencurrents are used in running the PLATE code. Our modeling result converged at a discretization of 8×8 cells. We can see a good match between the results of the two programs, but HFSHEET shows slightly larger values especially in the real component. Incident electric fields and the distribution of the surface scattering currents on the sheets are shown in Figure 3. The incident fields show a radiating pattern resulting from the vertical magnetic dipole source. Since we consider electrical permittivity as well as conductivity, the real part of the incident field exists, although it is very small. Since the sheet is surrounded by free space, conduction or channeling currents do not exist, so the scattering current forms a vortex on the surface of the sheet.

The next step is to test the accuracy at high frequencies where it is necessary to consider displacement currents. However, the lack of thin-sheet modeling in that frequency range led us to compare the results with those of the EM1D code (Pellerin et al., 1995). Figure 4 shows the model used for the comparison and resulting EM fields. We locate the vertical magnetic dipole source of unit moment at 2 m below the surface and the observation position at 8 m below surface and 2 m from

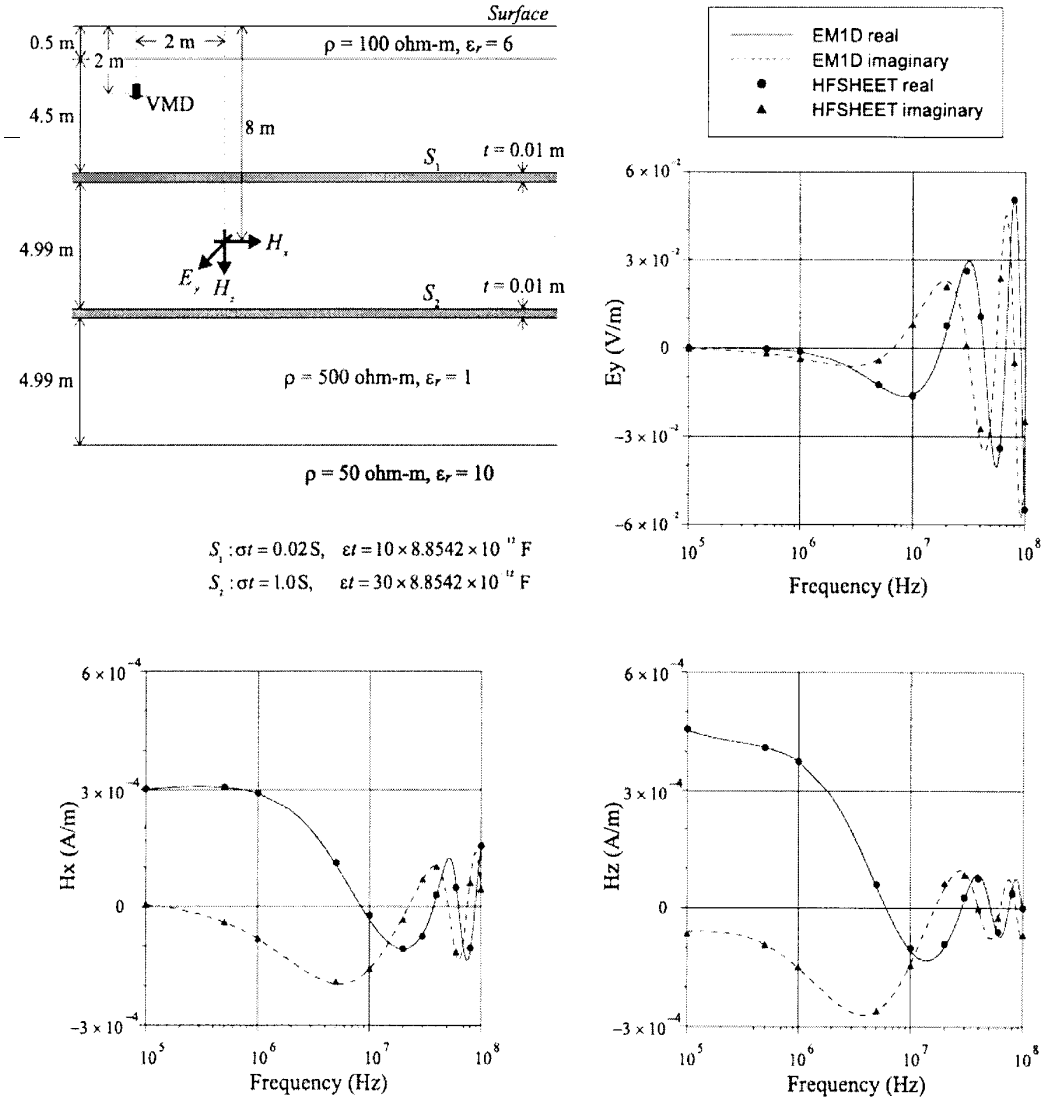

FIG. 4. High-frequency responses compared with EM1D (Pellerin et al., 1995). Upper left shows the model, including two thin, conductive sheets embedded in a three-layer earth (not exact in scale). In EM1D, the sheets are simulated with thin layers 0.01 m thick. For HFSHEET, the size of each sheet is 20×20 m for frequencies <10 MHz, divided by 10×10 cells, and is 10×10 m for frequencies >10 MHz, divided by maximum 18×18 cells. The vertical magnetic dipole source of unit moment is located above the center of the sheets.

the source. In such a configuration, received EM fields would show varying responses of the layered earth and sheets according to the frequency changes. The resulting EM fields shown contain the total field. The earth is composed of three layers: a thin overburden 0.5 m thick, a 14.5-m-thick host, and a conductive basement. The layer resistivities are $\rho_1 = 100$, $\rho_2 = 500$, and $\rho_3 = 50$ ohm-m, while the dielectric constants are 6, 1, and 10, respectively. The conductance and the product of the thickness and electric permittivity of S_1 are 0.02 S and $10 \times 8.8542 \times 10^{-12}$ F, respectively, while those of S_2 are 1.0 S and $30 \times 8.8542 \times 10^{-12}$ F, respectively. For the EM1D computation, the sheets are simulated by thin layers of 0.01 m thickness. For HFSHEET, the horizontal dimensions of the sheets are 20×20 m with 100 cells for frequencies < 10 MHz. At higher frequencies we use 10×10 m sheets with cell division of a maximum of 18×18 cells. The source is located directly above the center of the sheets.

At low frequencies where diffusion dominates, EM fields mostly show the response of the layered earth and the conductive lower sheet S_2. As the frequency is increased, the upper sheet S_1 starts to play an increasingly important role. Toward the high-frequency end wave propagation dominates diffusion, so we see characteristic fluctuations as a function of frequency. Throughout the entire frequency range, HFSHEET results match very well with the EM1D result. Both results shown above indicate HFSHEET produces accurate EM responses of the sheets throughout the frequency range from diffusion to wave propagation regime and for the wide range of host property—even for free space.

EXAMPLES FOR PLANE-WAVE EXCITATION

We tested HFSHEET using a two-sheet model with a plane-wave source. The test was made for conventional magnetotellurics and the high-frequency impedance method (Song et al., 2002). Figure 5 shows the model used to compute magnetotelluric (MT) responses. Two conductive sheets, one vertical and the other dipping, with conductance of 10 S are embedded in a three-layer earth. Operating frequencies range from 10^{-3} to 10^4 Hz, with four frequencies per decade in logarithmic scale. Figures 6 and 7 show the apparent resistivity and phase pseudosections for TE- and TM-mode excitations, respectively. The results are shown only for the frequencies from 10^{-2} to 10^3 Hz since there is no anomaly apparent in the section beyond this frequency range. We can see clear responses of the conductive sheets, both in apparent resistivity and phase sections in TE mode (Figure 6). The dip of the inclined sheet is hardly resolved in the apparent resistivity section, while we can infer it from the subtle asymmetric pattern in the phase section. In TM mode, on the other hand, we can see no response of the

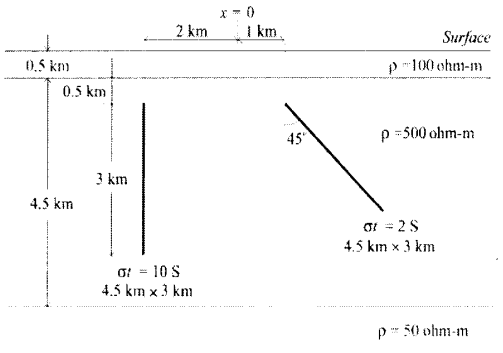

FIG. 5. Two thin conductors embedded in a three-layer earth. Four frequencies per decade are used from 0.01 to 1000 Hz in the MT modeling.

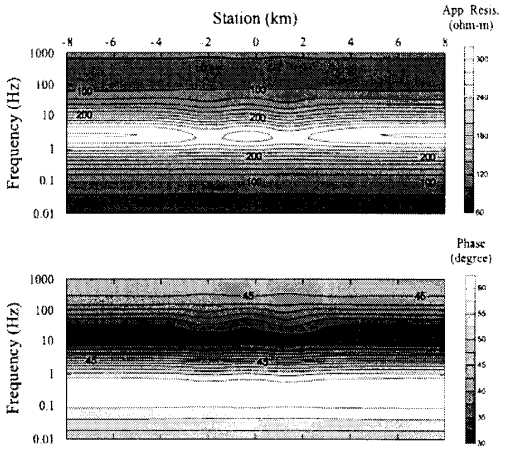

FIG. 6. Apparent resistivity (upper) and phase (lower) sections of the TE-mode MT impedance Z_{yx} for the model in Figure 5. Two conductive sheets are easily separated in the upper and lower sections, although the attitude of the dipping sheet is not apparent.

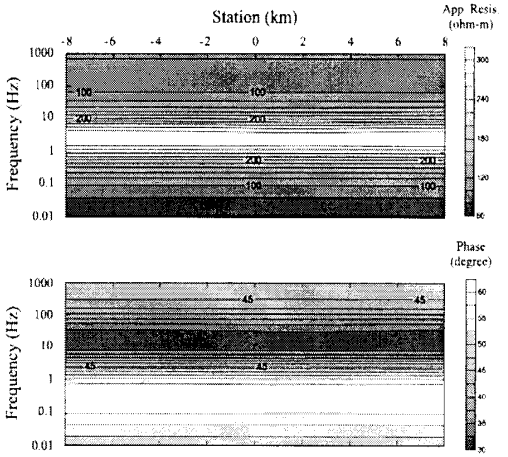

FIG. 7. Apparent resistivity (upper) and phase (lower) sections of the TM-mode MT impedance Z_{xy} for the model in Figure 5. The vertical sheet is undetectable in TM mode where the primary and measuring electric field directions are normal to the sheet. The dipping sheet shows only very weak anomaly beneath the station at 2 km, which corresponds to its center.

sheets either in the apparent resistivity or in the phase pseudosection. A slight anomaly exists beneath the station at 2 km, which corresponds to the center of the dipping sheet.

In TM mode excitation there are neither incident electric fields nor the scattering currents on the vertical sheet alone. However, there does exist a scattering current in the vertical sheet as a result of coupling with the dipping sheet. Figure 8 shows incident electric fields on the dipping sheet and scattering currents in the dipping and the vertical sheets at 10 Hz frequency for the results shown in Figure 7. The polarity change in the imaginary part of the incident electric fields says the center of the dipping sheet is at about one skin depth. Current channeling plays a major role in the scattering current, but we can still see the vortex current in the imaginary part in the dipping sheet. As shown in Figure 8c, the scattering current in the vertical sheet is considerable despite the absence of incident or exciting electric fields. Much of the secondary electric field as the result of the vertically dominant scattering current cancels out along the profile axis, so we cannot see any anomaly attributable to the vertical sheet.

Figure 9 shows another model for the high-frequency impedance method (Song et al., 2002). The impedance measurement technique offers an attractive opportunity for imaging near-surface conductivity and dielectric constant in that we are free from source coupling, which is difficult to determine at high frequencies. The geometry in Figure 9 is 1–500 scaled from that shown in Figure 5: two conductive sheets in a three-layer earth of which the dielectric constants are newly assigned. In the high-frequency range, sheets must be defined in terms of admittance and not just conductance. The two sheets have different admittances from each other, primarily because of electrical permittivity. Operating frequencies range from 10 kHz to 100 MHz, covering the conventional diffusion and wave propagation regimes. Note that for the wave propagation region, we use linearly increased frequencies; an exponential spacing is used for low frequency.

For a homogeneous half-space, the amplitude of impedance increases with the square root of frequency below the frequency, or $\omega_T = \sigma/\varepsilon$ (Annan, 1996). For frequencies higher than ω_T, the amplitude turns flat and becomes independent

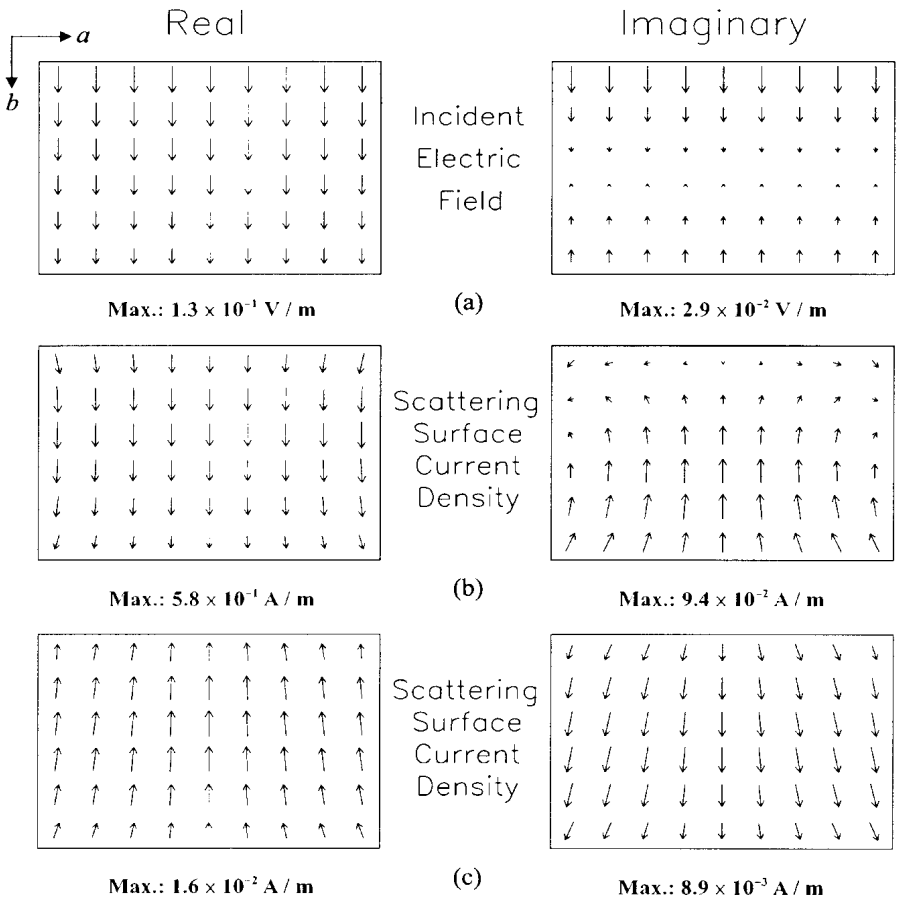

FIG. 8. The amplitudes and directions of (a) the incident electric fields on the dipping sheet, (b) scattering surface current densities on the dipping sheet, and (c) scattering surface current densities on the vertical sheet at 10 Hz frequency shown in Figure 7. The scattering currents can be seen on the vertical sheet, although there are no incident electric fields on it for TM mode, which results from coupling with the dipping sheet.

of frequency. The phase change takes place over a wider band, from 45° in diffusion to 0° in wave propagation regimes. For a layered earth, the interference between multiple reflections in a layer makes the impedance oscillate as the frequency changes (Song et al., 2002). Figure 10 shows the amplitude and phase curves of the impedance on the surface of the layered earth shown in Figure 9 for normal incidence. We can see from the amplitude curve that ω_T is about 1 MHz. Two kinds of oscillation start from 3 MHz; they are clearer in the phase curve. The highly oscillatory feature results from the interference of reflections trapped in the top layer, while the broader oscillation indicates the reflections trapped in the middle layer.

The impedance response for the sheet model is expected to show these oscillations as in the amplitude and phase of impedance sections for TE mode incidence (Figure 11). The amplitude and phase show induction responses of the sheets for frequencies <10 MHz, and we can identify the dipping sheet from the asymmetric anomalies both in the amplitude and phase sections. For frequencies >10 MHz, the broad oscillation in Figure 10 is observed but the highly oscillatory feature is not seen. We can also see small periodic anomalies, which result from the multiples of diffracted energy from the edges of the sheets. In TM mode response (Figure 12) we cannot see an anomaly of the vertical sheet, but the response of the dipping sheet is clear both in the amplitude and phase of impedance

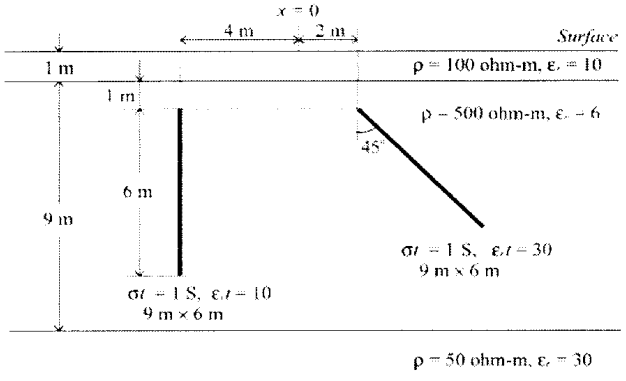

FIG. 9. Two-sheet model for high-frequency impedance application. All the geometrical parameters are scaled by 1/500 from those in Figure 5. Both the resistivities and the electric permittivities are assigned to the layers since displacement currents have an effect on the EM responses at the high-frequency range. The electrical properties of the sheets should be considered as admittance rather than conductance. Nineteen frequencies from 10 kHz to 100 MHz, with a logarithmic sampling of frequencies <10 MHz and every 10 MHz above that, are used in the modeling.

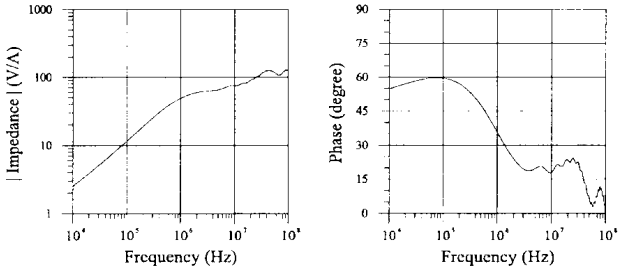

FIG. 10. Amplitude (left) and phase (right) curves of the impedance for normal incidence on the layered earth shown in Figure 9 without the two sheets. For frequencies <1 MHz, the amplitude increases with the square root of frequency. Two kinds of oscillatory feature are seen at high frequencies, which result from the interference of multiple reflections trapped in each layer.

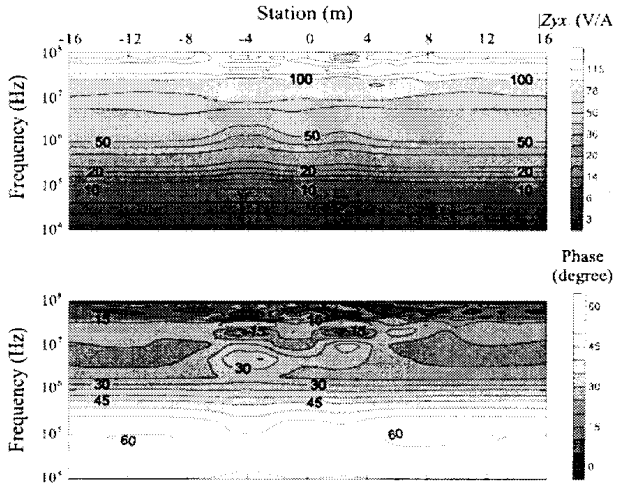

FIG. 11. Amplitude (upper) and phase (lower) sections of the TE-mode impedance Z_{yx} for the model shown in Figure 9. The induction responses of the two sheets can be seen for frequencies <10 MHz, while for higher frequencies the wave propagation phenomena are mixed up with the oscillation for the layered earth shown in Figure 10.

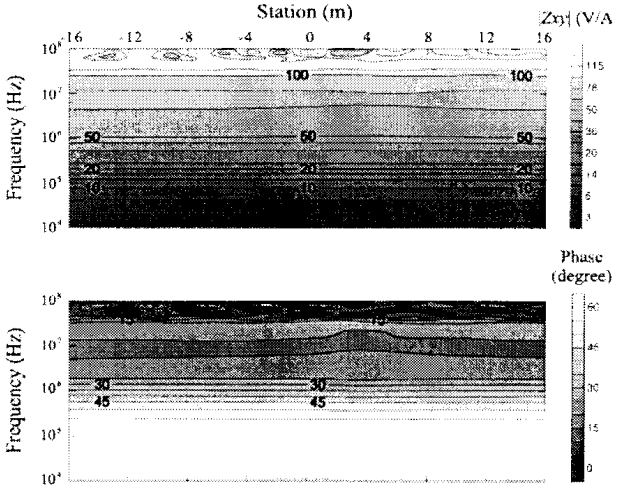

FIG. 12. Amplitude (upper) and phase (lower) sections of the TM-mode impedance Z_{xy} for the model shown in Figure 9. Only the induction responses of the dipping sheet can be seen for frequencies between 1 and 10 MHz, and periodic anomalies associated with wave propagation are visible for frequencies >30 MHz.

sections. We can identify again the propagating phenomena of diffracted energy mixed with the broader oscillation above 30 MHz. The oscillating feature of impedance for the layered earth will not have an effect on the analysis when the 1-D inversion including displacement currents is applied, even for the oblique incidence of plane wave (Song et al., 2002). However, the resonance associated with the propagation of diffracted or reflected energy from the isolated body must be handled with a higher-dimension inversion tool to produce an accurate analysis of the subsurface structure.

CONCLUSIONS

We have developed a wide-band, thin-sheet EM modeling scheme using the integral equation method. The approach is based on Weidelt's (1981) work. Additional features in our development involve inclusion of the displacement currents in the formulation, analytic treatment of the singular cell integral of Green's function, and generalization of the formulation with the tensor notation. The model is composed of two sheets embedded in a three-layer earth. The source field can be generated by a remote or local electric or magnetic dipole source on the surface or in a borehole. The conductivity and electrical permittivity of the host medium and sheets can be arbitrary and dispersive.

The accuracy of the HFSHEET code has been verified over a wide range of frequencies and host medium properties. The HFSHEET code is also used to investigate plane-wave responses of the two-sheet model in a three-layer earth. In analyzing the MT responses, we can clearly identify the coupling between the vertical and dipping sheets by observing the scattering currents in the vertical sheet. In the presence of a TM mode plane-wave source field, no current would exist in the vertical sheet. In modeling high-frequency impedance, we identify characteristic responses of the layered earth and sheets as the frequency increases from the diffusion range to the wave propagation regime.

For accurate evaluation of the Hankel transform involved in computing Green's functions for a layered earth, we used a Gaussian quadrature. The integral is divided into two regions, one to left of the branch point and the other to the right. As we increase the frequencies, more sampling in the horizontal wavenumber is required, resulting in a linear increase in computing time.

ACKNOWLEDGMENTS

This work was partially supported by U.S. EPA contract DW89937618-01-3 and partially by the Director, Office of Energy Research, Office of Basic Energy Sciences, Engineering and Geosciences Division of the U.S. Department of Energy under contract DE-AC-03-76SF00098. We thank B. S. Singer for his valuable comments on the singular Green's function integral.

REFERENCES

Annan, A. P., 1974, The equivalent source method for electromagnetic scattering analysis and its geophysical application: Ph.D. thesis, Memorial Univ. of Newfoundland.

———1996, Transmission, dispersion and GPR: J. Environ. Eng. Geophys., **0**, 125–136.

Chave, A. D., 1983, Numerical integration of related Hankel transforms by quadrature and continued fraction algorithm: Geophysics, **48**, 1671–1686.

Cole, K. S., and Cole, R. H., 1941, Dispersion and adsorption in dielectrics: J. Chem. Phys., **9**, 341–351.

Dyck, A. V., Bloore, M., and Vallee, M. A., 1980, User manual for programs PLATE and SPHERE: Res. Appl. Geophys., **14**.

Fainberg, E. B., Pankratov, O. V., and Singer, B. S., 1993, Thin sheet modelling of subsurface and deep inhomogeneities: Geophys. J. Internat., **113**, 144–154.

Joshi, M. S., Gupta, O. P., and Negi, J. G., 1988, On the effects of thickness of the half-plane model in HLEM induction prospecting over sulphide dykes in a highly resistive medium: Geophys. Prosp., **36**, 551–558.

Lajoie, J. J., and West, G. F., 1976, The electromagnetic response of a conductive inhomogeneity in a layered earth: Geophysics, **41**, 1133–1156.

Pellerin, L., Labson, V. F., and Pfeifer, M. C., 1995, VETEM—A very early time electromagnetic system: Symposium on the Application of Geophysics to Engineering and Environmental Problems (SAGEEP), Proceedings, 725–731.

Price, A. T., 1949, The induction of electric currents in non-uniform thin sheets and shells: Quart. J. Mech. and App. Math., **2**, 283–310.

Song, Y., Kim, H. J., and Lee, K. H., 2002, High-frequency electromagnetic impedance method for subsurface imaging: Geophysics, **67**, 501–510.

Vasseur, G., and Weidelt, P., 1977, Bimodal electromagnetic induction in non-uniform thin sheets with an application to the northern Pyrenean induction anomaly: Geophys. J. Roy. Astr. Soc., **51**, 669–690.

Walker, P. W., and West, G. W., 1991, A robust integral equation solution for electromagnetic scattering by a thin plate in conductive media: Geophysics, **56**, 1140–1152.

Ward, S. H., and Hohmann, G. W., 1988, Electromagnetic theory for geophysical applications, *in* Nabighian, M. N., Ed., Electromagnetic methods in applied geophysics, **1**: Soc. Expl. Geophys., 131–312.

Weidelt, P., 1981, Report on dipole induction by a thin plate in a conductive halfspace with an overburden: Fed. Inst. Earth Sci. and Mate. Report 89727.

Zhou, Q., 1989, Audio-frequency electromagnetic tomography for reservoir evaluation: Ph.D. thesis, Univ. of California.